

Regular Article -Theoretical Physics

T-matrix analysis of static Wilson line correlators from lattice QCD at finite temperature

Zhanduo Tang^{1,a}, Swagato Mukherjee², Peter Petreczky², Ralf Rapp¹

Overlotron Institute and Department of Physics and Astronomy, Texas A&M University, College Station, TX 77843-3366, USA

Received: 17 November 2023 / Accepted: 2 April 2024 / Published online: 25 April 2024

© The Author(s), under exclusive licence to Società Italiana di Fisica and Springer-Verlag GmbH Germany, part of Springer Nature 2024
Communicated by Laura Tolos

Abstract We utilize a previously constructed thermodynamic T-matrix approach to the quark-gluon plasma (QGP) to derive constaints on its input by using results on Wilson line correlators (WLCs) of a static quark-antiquark pair from 2 + 1-flavor lattice-QCD (lQCD) computations with realistic pion mass. The self-consistent T-matrix results, which include previous constraints from the IQCD equation of state in the light-parton sector, can describe the IQCD data for WLCs fairly well once refinements of its driving kernel are applied. In particular, the input potential requires less screening than what has been inferred from previous T-matrix analyses. Pertinent predictions for the spectral and transport properties of the QGP are discussed, including the spatial diffusion coefficient for heavy quarks; the latter turns out to have a rather weak temperature dependence, in approximate agreement with recent unquenched IQCD results.

1 Introduction

The study of the quark-gluon plasma (QGP) provides unique opportunities to understand how emergent many-body phenomena arise from the fundamental interactions between the partons in Quantum Chromodynamics (QCD). In particular, heavy-flavor (HF) particles are widely regarded as excellent probes of the transport and hadronization properties of the QCD medium produced in ultrarelativistic heavy-ion collisions (URHICs) [1–3], for several reasons. Heavy quarks and antiquarks (Q and \bar{Q}) are pairwise produced in initial hard processes and approximately conserved throughout the evolution of fireball. Their subsequent propagation through the medium can be characterized by well-defined transport coefficients, most notably the spatial diffusion coefficient. The interactions between heavy quarks and the medium occur

with small energy transfer and thus enable the use of potential approximations. The spectra of HF particles can preserve a memory of their interaction history as their thermalization time, which is parametrically enhanced by their massover-temperature ratio, is comparable to or (for bottom) even longer than the fireball lifetime.

Bound states of heavy quark and antiquark, i.e., quarkonia, provide further insights into the properties of the QGP in URHICs [4–6], as their in-medium properties are closely related to the in-medium QCD force. These properties fundamentally figure in the transport coefficients which govern the abundance and transverse-momentum spectra of quarkonia [7]. For example, quarkonia kinetics critically depends on their inelastic reaction rates, which, in turn, depend on the in-medium binding energies and are closely related to individual heavy-quark (HQ) interactions with the medium. Lattice-QCD (IQCD) computations have provided ample information on the in-medium properties of heavy quarkonia through HQ free energies and Euclidean correlators [8-25] which constrain the spectral functions that can be computed in effective models and that subsequently serve as an input to phenomenological applications [26–28].

In the present paper we focus on Wilson line correlators (WLCs) of a static quark-antiquark pair at finite temperature. Pertinent IQCD results have recently been obtained using realistic 2+1-flavor IQCD calculations [29]. When compared to predictions from hard-thermal loop (HTL) perturbation theory, a marked disagreement was found. On the other hand, when using schematic spectral functions based on parametrizations with different ansätze, it was inferred that the underlying potential exhibits a relatively weak screening, even at rather large distances, while the widths of the spectral peaks turned out to be substantial, albeit quantitatively with a rather large spread. These results were refined and essentially confirmed in a more recent analysis [30]. Clearly, these findings call for microscopic analysis within a nonperturbative



² Physics Department, Brookhaven National Laboratory, Upton, NY 11973, USA

^a e-mail: zhanduotang@tamu.edu (corresponding author)

92 Page 2 of 12 Eur. Phys. J. A (2024) 60:92

approach. Toward this end, we will employ quantum many-body theory, *i.e.*, a thermodynamic T-matrix approach, that has been previously constructed to describe the interactions between partons in a strongly coupled QGP [31,32]. Utilizing a Hamiltonian with a non-perturbative input potential [33], the 1- and 2-body correlation functions are evaluated selfconsistently [34–36]. In the vacuum, the kernel reduces to the standard Cornell potential, while its finite-temperature corrections have been constrained by IQCD data for the HQ free energy and equation of state (EoS). The WLCs from IQCD provide a novel opportunity to improve the constraints on the in-medium potential, especially since their dependence on euclidean time, τ , for different values of spatial separation, r, provides a much extended dynamical reach compared to the HQ free energies which are evaluated at $\tau = 1/T$.

The remainder of this article is structured as follows. In Sect. 2, we briefly recollect the key components of the thermodynamic *T*-matrix approach as needed in the present context, in particular its driving kernel (potential) as the main input quantity. In Sect. 3 we discuss how the pertinent static quarkonium spectral function can be related to the WLCs computed on the lattice. The new constraints imposed on the in-medium corrections to the potential from selfconsistent fits to the IQCD data for EoS and the first moment of the static WLCs are elaborated in Sect. 4. In Sect. 5 we compute the transport coefficients of charm and static quarks predicted by the newly inferred potential and compare the diffusion coefficient to recent IQCD results. Our summary and conclusions are contained in Sect. 6.

2 T-matrix approach

The thermodynamic *T*-matrix is a quantum many-body formalism to evaluate 1- and 2-body correlation functions self-consistently by resumming an infinite series of selfenergy and ladder diagrams; thus, it is suitable to study both bound and scattering states for strongly interacting systems. Originally devised for the study of HF particles within the QGP context [31,32,34], this approach was subsequently extended to encompass the light-parton sector [37]. By reducing the 4-dimensional (4D) Bethe-Salpeter equation into a more manageable 3D Lippmann-Schwinger equation [38], followed by a partial-wave expansion, one obtains a 1D scattering equation [36,37],

$$T_{ij}^{L,a}(z, p, p') = V_{ij}^{L,a}(p, p') + \frac{2}{\pi} \int_{-\infty}^{\infty} k^2 dk V_{ij}^{L,a}(p, k) \times G_{ij}^0(z, k) T_{ij}^{L,a}(z, k, p')$$
(1)

that features the intermediate 2-parton propagator,



$$G_{ij}^{0}(z,k) = \int_{-\infty}^{\infty} d\omega_1 d\omega_2 \frac{\left[1 \pm n_i (\omega_1) \pm n_j (\omega_2)\right]}{z - \omega_1 - \omega_2}$$
$$\times \rho_i (\omega_1, k) \rho_j (\omega_2, k) \tag{2}$$

which is a convolution of two single-parton spectral functions.

$$\rho_i(\omega, k) = -\frac{1}{\pi} \operatorname{Im} G_i(\omega + i\epsilon, k)$$
(3)

given in terms of the (positive-energy projected) propagators,

$$G_i(\omega, k) = 1/[\omega - \varepsilon_i(k) - \Sigma_i(k)]. \tag{4}$$

In Eq. (1), $V_{ij}^{L,a}$ denotes the potential between particle i and j in a color channel a with angular momentum L, the n_i are Bose (+) or Fermi (-) distribution functions, $\varepsilon_i = \sqrt{M_i^2 + k^2}$ on-shell energies with particle mass $M_i = -\frac{1}{2} \int \frac{d^3 \mathbf{p}}{(2\pi)^3} V_{ii}^{a=1}(\mathbf{p}) + M_i^0$, composed of a selfenergy part from the color-singlet (a=1) potential ("Fock term") and a bare mass, M_i^0 , and p and p' are the moduli of incoming and outgoing momenta in the center-of-mass (CM) frame. The in-medium 1-particle selfenergies, $\Sigma_i(k)$, in Eq. (4) are calculated by closing the T-matrix with an in-medium 1-parton propagator [36,37].

The ansatz for the static in-medium potential in colorsinglet state is taken from Ref. [33], whose Fourier transform yields a screened Cornell potential,

$$\widetilde{V}(r,T) = -\frac{4}{3}\alpha_s \left[\frac{e^{-m_d r}}{r} + m_d \right] - \frac{\sigma}{m_s} \left[e^{-m_s r - (c_b m_s r)^2} - 1 \right].$$
(5)

In vacuum one recovers the standard form, $\widetilde{V}(r) = -\frac{4}{3} \frac{\alpha_s}{r} +$ σr , where the coupling constant $\alpha_s = 0.27$ (including an offshell running [32]) and string tension, $\sigma = 0.225 \text{ GeV}^2$, are fitted to the vacuum free energy from IQCD data [21,27,39-42], assuming a string breaking distance of $r_{SB} = 1$ fm. For the in-medium potential, m_d and m_s are the Debye screening masses for color-Coulomb and confining interactions [37]; an additional parameter c_h in the quadratic term of the exponential of the confining term has been introduced to control its saturation at large r, essentially mimicking in-medium string breaking. The infinite-distance subtracted potential, $V(r,T) = \tilde{V}(r,t) - \tilde{V}(\infty,T)$, is then Fourier transformed; for the interactions between particles with finite masses, the static potential in momentum space acquires relativistic corrections induced by the underlying Lorentz structure [32], resulting in

$$V_{ij}\left(\mathbf{p},\mathbf{p}'\right) = \mathcal{R}_{ij}^{vec} V^{vec}\left(\mathbf{p} - \mathbf{p}'\right) + \mathcal{R}_{ij}^{sca} V^{sca}\left(\mathbf{p} - \mathbf{p}'\right)$$
(6)

where V^{vec} (V^{sca}) denotes the static vector (scalar) potential. One has Eur. Phys. J. A (2024) 60:92 Page 3 of 12 92

$$\mathcal{R}_{ij}^{vec} = \sqrt{1 + \frac{p^2}{\varepsilon_i(p)\varepsilon_j(p)}} \sqrt{1 + \frac{p'^2}{\varepsilon_i(p')\varepsilon_j(p')}}$$
(7)

$$\mathcal{R}_{ij}^{sca} = \sqrt{\frac{M_i M_j}{\varepsilon_i(p)\varepsilon_j(p)}} \sqrt{\frac{M_i M_j}{\varepsilon_i(p')\varepsilon_j(p')}}.$$
 (8)

The color-Coulomb potential is characterized by an entirely Lorentz vector structure, while the confining potential is commonly assumed to be scalar [43,44], in which case $V^{vec} = V_C$ and $V^{sca} = V_S$. However, in Refs. [45–49] it has been suggested that the confining potential exhibits a combination of vector and scalar Lorentz structures, expressed as $V^{vec} = V_C + (1 - \chi)V_S$ and $V^{sca} = \chi V_S$, rather than being exclusively scalar. In this context, the key parameter is the mixing coefficient, χ , wherein $\chi = 1$ represents a purely scalar confining potential, and values below one admix a vector component. In a previous study of $1/m_O$ corrections (m_O : HQ mass) to the HQ interaction [36] we have found that a mixing coefficient of $\chi = 0.6$ leads to a marked improvement of the spin-orbit and spin-spin splittings in vacuum charmonium and bottomonium spectroscopy [50] over the $\chi=1$ case. In addition, the resulting charm-quark diffusion coefficient showed better agreement with 2+1-flavor IQCD data [51]. Therefore, we also introduce the mixing effect in this study. Finally, we note that the potential is extended to different color channels, denoted by a in Eq. (1), using pertinent Casimir coefficients [36,37].

3 Static Wilson line correlators from the *T*-matrix

The static Wilson line correlator in Euclidean time, which is amenable to IQCD computations, is connected to the static $Q\bar{Q}$ spectral function $\rho_{Q\bar{Q}}$, through a Laplace transform,

$$W(r,\tau,T) = \int_{-\infty}^{\infty} dE e^{-E\tau} \rho_{Q\bar{Q}}(E,r,T), \qquad (9)$$

where r is the distance between Q and \bar{Q} , and E their total energy which is measured relative to the mass threshold of the bare HQ mass, $2M_Q^0$ (numerically taken as 2×10^4 GeV). The constituent static HQ mass is the sum of the bare mass and the mass shift originating from the selfenergy, *i.e.*, $M_Q = M_Q^0 + \tilde{V}(r \to \infty)/2$ [37]. The inversion of Eq. (9) is a challenging (if not ill-posed) problem, making it difficult to reconstruct spectral functions from IQCD results for WLCs. On the other hand, if one can calculate the WLCs with spectral functions obtained from an effective model using Eq. (9), the comparison of the model-derived WLCs with lattice data can test the model capabilities and provide microscopic insights.

In the T-matrix formalism, the $Q\bar{Q}$ spectral function takes the same form as given in Ref. [37],

$$\begin{split} & \rho_{Q\bar{Q}}\left(E,r,T\right) \\ & = \frac{-1}{\pi} \mathrm{Im} \left[\frac{1}{E - \widetilde{V}(r,T) - \Phi(r,T) \Sigma_{Q\bar{Q}}(E,T)} \right] \end{split} \tag{10}$$

where $\widetilde{V}(r,T)$ is the static in-medium potential introduced in Sect. 2. The two-body selfenergy, $\Sigma_{Q\bar{Q}}$, is related to the two-body propagator by

$$\left[G_{Q\bar{Q}}^{0}(E)\right]^{-1} = E - \widetilde{V}(r \to \infty) - \Sigma_{Q\bar{Q}}(E). \tag{11}$$

The two-body selfenergy is reduced by interference effects that depend on the relative distance between the quarks and are sometimes referred to as the "imaginary part of potential" [52]. In the T-matrix formalism, these correspond to 3body diagrams, which are difficult to calculate explicitly [37]. However, one can approximately implement them through an r-dependent suppression factor (or interference function), $\phi(r)$ [37], i.e., $\Sigma_{O\bar{O}}(E,r) = \Sigma_{O\bar{O}}(E)\phi(r)$. In perturbation theory, $\phi(r)$ has been calculated, essentially corresponding to an atanh-function (which vanishes for $r \to 0$ in the colorsinglet channel and goes to 1 for $r \to \infty$) [52]. In a nonperturbative setting, it has been supplemented with an extra stretch-factor in the argument, which has been determined via IQCD constraints from static free energies [37]. The interference effect is expected to be significant for deeply bound heavy quarkonia and has been found to improve the description of Euclidean quarkonium correlator ratios within the T-matrix approach [37].

To facilitate the understanding of the physical meaning of the lattice results for the WLCs and to what extent these can constrain the $Q\bar{Q}$ spectral function, n^{th} -order cumulants have been defined in Ref. [29] as

$$m_1(r, \tau, T) = -\partial_\tau \ln W(r, \tau, T)$$
(12)

$$m_n = \partial_{\tau} m_{n-1}(r, \tau, T), n > 1.$$
 (13)

The first cumulant, m_1 , essentially corresponds to an effective mass that is commonly used in lattice QCD. In general, the WLC contains many states at T=0. At large τ (i.e., small energies) it will be dominated by the ground state that defines the potential at zero temperature. At higher energies, excited states contributing to the WLC are related to hybrid potentials (such as those between D-mesons) which will cause m_1 to have a rather complex behavior at small τ . At non-zero temperature, where only data at relatively small τ are available, this fact renders the analysis quite involved. On the other hand, the contribution of the high-energy part of the spectral function is temperature independent to a fairly good approximation [29]. This contribution can then be estimated using T=0 lattice results for WLCs and subtracted from the

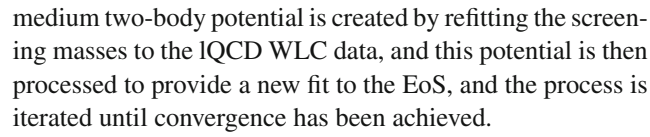


finite-temperature results. In practice one can calculate the first cumulant of the subtracted WLC, m_1^{sub} , which will be sensitive to the dominant peak in the spectral function, *i.e.*, to the potential, for sufficiently small τ . Therefore, we employ the lQCD results for m_1^{sub} , where the high-energy contribution to the WLC has been subtracted, following the procedure outlined in Ref. [29], and focus on its small τ behavior. Using m_1^{sub} has also another advantage: typically lattice results for correlators for small τ suffer from discretization effects, which cause distortions of the corresponding spectral function at large energies, see, *e.g.*, the discussion in Ref. [53]. Since the high-energy part of the spectral function is subtracted when evaluating m_1^{sub} , the small τ behavior of m_1^{sub} is free of lattice artifacts.

Returning to the T-matrix expression, Eq. (10), one can show by expanding m_1^{sub} for $\tau \to 0$ and considering the analytic properties of the two-body selfenergy, that $m_1(r,\tau=0,T)$ reduces to the potential $\widetilde{V}(r,T)$, see Appendix A for more details (this also holds in the perturbative HTL approach). The second cumulant m_2^{sub} of the subtracted WLC, or equivalently the slope of m_1^{sub} , is related to the imaginary part (width) figuring in $\rho_{Q\bar{Q}}$, characterizing the interacting strength between $Q\bar{Q}$ and medium. Since we only consider subtracted cumulants in this study, the superscript sub will be omitted in what follows.

4 In-medium potentials constrained by IQCD

In this section, we lay out the procedure of inferring the modifications to the in-medium potential utilizing combined fits of quarkonim spectral function to the WLCs and of the light-parton properties to the QGP EoS in a selfconsistent quantum many-body approach [36,37]. The procedure consists of two selfconsistency loops, as follows. Initially, the parameterization of the in-medium potential is refined using the cumulants of static WLCs (m_1) obtained from the Tmatrix approach and fitting them to the IQCD data. The fit parameters in this step are the screening masses, m_d (color-Coulomb) and m_s (confining), as well as c_b which controls the "string breaking". Subsequently, these refined in-medium potentials are used to compute the EoS of QGP, and the main parameters in this step include the in-medium light-quark and gluon masses. Since the calculation of EoS requires the onebody spectral functions and two-body scattering amplitudes (which depend on each other through the parton selfenergies, cf. Eqs. (1)–(4)), one has to solve a selfconsistency problem which is done by numerical iteration. The selfenergies of the heavy quarks, calculated from heavy-light T-matrices closed off with thermal parton spectral functions, are then reinserted into the calculation of the WLCs via Eq. (9) using the inmedium quarkonium spectral functions. A further refined in-



In the remainder of this section, we discuss our numerical fits of the EoS (following Ref. [37]) in Sect. 4.1 and the results for the WLCs in Sect. 4.2.

4.1 Equation of state

The equation of state is encoded in the pressure, $P(T, \mu)$, of a many-body system as a function of temperature and chemical potential(s). In the present context, IQCD data for the EoS are used to adjust the bare light-parton masses which are due to effects that are not explicitly part of the many-body calculations, e.g., due to quark or gluon condensates (similar to what is done in quasiparticle models). In the grand canonical ensemble the pressure is related to the grand potential per unit volume via $\Omega = -P$. For an interacting system, it can be calculated diagrammatically within the Luttinger-Ward-Baym (LWB) formalism where all closed-loop "skeleton" diagrams are computed with fully dressed propagators [54–56], also referred to as a 2-particle irreducible approach. This constitutes a conserving (i.e., thermodynamically consistent) approximation scheme, which is compatible with the ladder resummation in the selfconsistent T-matrix and selfenergies. Formulated as a Hamiltonian approach to the QCD, this has been carried out in Refs. [37,57]. In particular, the Luttinger-Ward functional, Φ , could be resummed utilizing a matrix-logarithm resummation technique which accounts for the possibility of dynamically formed bound states contributing to the EoS. In compact form the result can be written

$$\Omega = \sum_{j} \mp d_{j} \int d\tilde{p} \left\{ \ln \left(-G_{j}(\tilde{p})^{-1} \right) + \left[\Sigma_{j}(\tilde{p}) - \frac{1}{2} \log \Sigma_{j}(\tilde{p}) \right] G_{j}(\tilde{p}) \right\},$$
(14)

using the notation $\int d\tilde{p} \equiv -\beta^{-1} \sum_n \int d^3 \mathbf{p}/(2\pi)^3$ with $\tilde{p} \equiv (i\omega_n, \mathbf{p})$ and $\beta = 1/T$. The summation in Eq. (14) includes all light-parton channels with the spin-color degeneracy d_j , and the \mp sign corresponds to bosons (upper) or fermions (lower). The three terms in Eq. (14), $\ln(-G^{-1})$, ΣG , and $\log \Sigma G$, correspond to the contributions from quasiparticles, selfenergies and the Luttinger-Ward functional (LWF) characterizing two-body interactions, respectively.

We present the fits to the pressure as obtained from lQCD [42] together with LWF contributions, as well as the corresponding light-parton masses in Fig. 1. In accordance with the findings in Refs. [36,37], the two-body interactions play an increasingly important role as temperature decreases, becoming the leading contribution at $T=0.195\,\text{GeV}$, indi-



Eur. Phys. J. A (2024) 60:92 Page 5 of 12 92

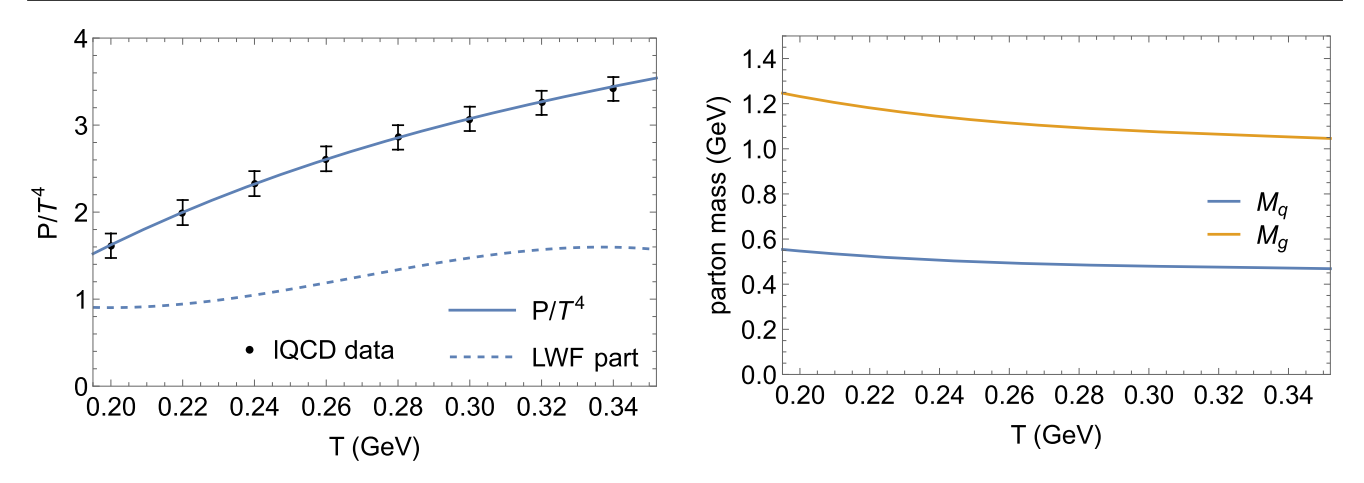


Fig. 1 Left panel: the pressure scaled by T^4 (blue line) compared to the pertinent 2+1-flavor IQCD data [42], as well as the LWF contribution (dashed line). Right panel: the total in-medium masses (i.e., bare plus selfenergies) for light quarks (blue) and gluons (orange) as a function of temperature

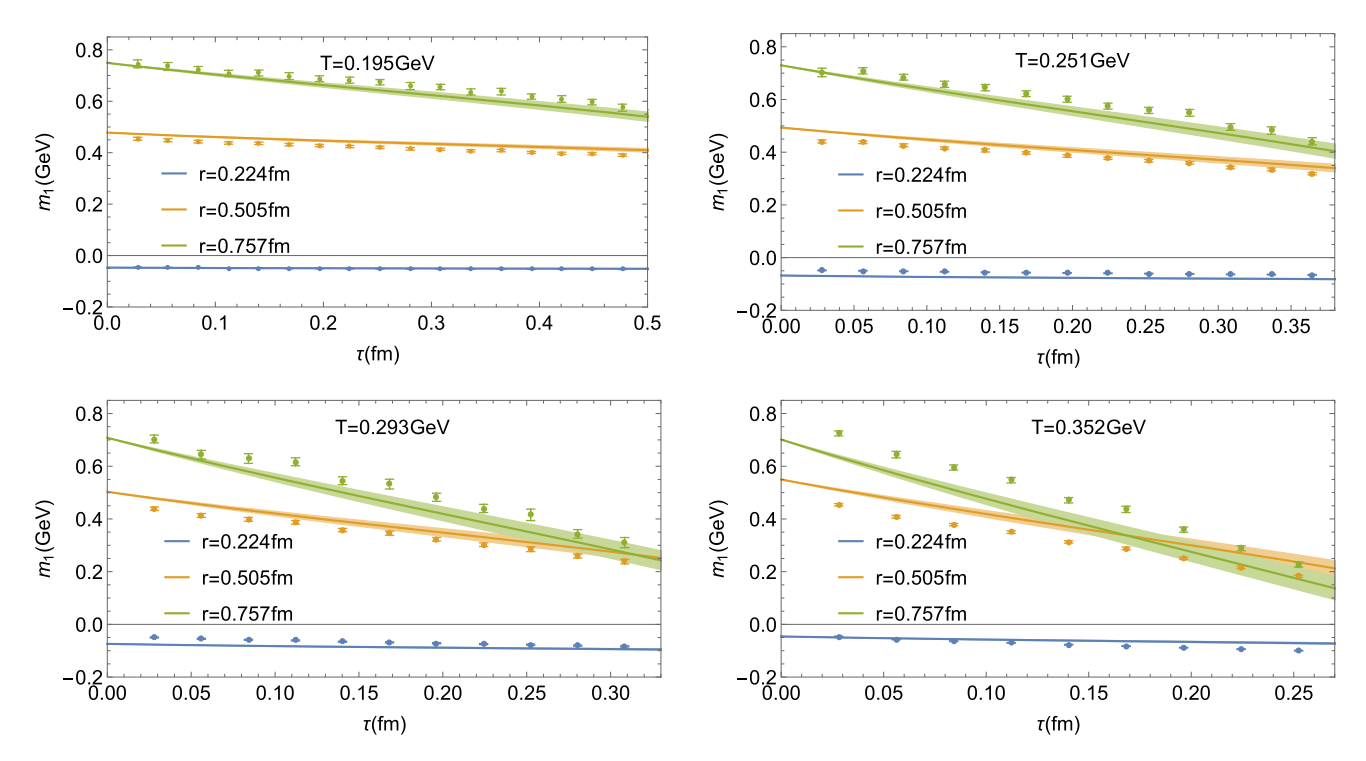


Fig. 2 The first cumulants of WLCs from the selfconsistent *T*-matrix results (lines) as a function of imaginary time at different temperatures and distances in comparison with the corresponding 2+1-flavor lQCD data [30]

cating a transition in the degrees of freedom (from partons to mesons and diquarks) in the system.

4.2 Static Wilson line correlators

Next we turn to the fits to the cumulants of the WLCs, which are, in fact, part of the combined fit procedure as outlined at the beginning of this section, cf. Fig. 2. We use the lQCD results on m_1 from Ref. [30]; since only the first cumulant was computed in that work we do not consider higher-order

cumulants here. We focus on the behavior of m_1 at small τ for reasons explained in Sect. 3. As also pointed out there lattice artifacts are not of concern even at small τ because we use subtracted cumulants. A fair overall agreement with the lQCD results can be achieved for both the intercept at $\tau \to 0$ and the slopes of m_1 , although the description somewhat worsens at the highest temperature. We will return to possible reasons for that below.

For the interference function, $\Phi(r, T)$, we simply took the results from previous work [37] (interpolated to the set



92 Page 6 of 12 Eur. Phys. J. A (2024) 60:92

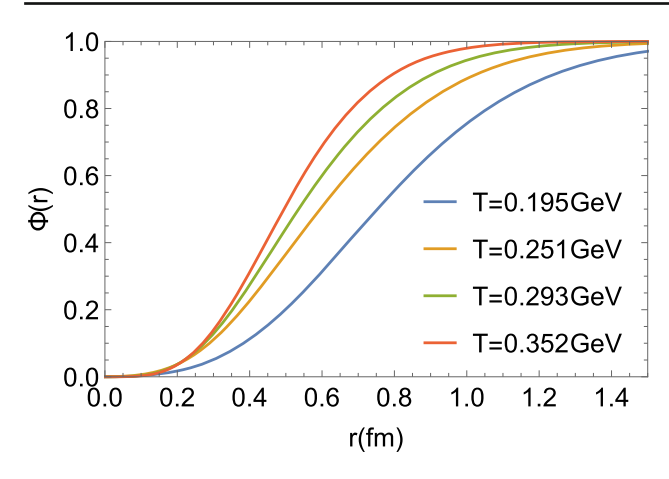


Fig. 3 The interference function, $\Phi(r)$, as a function of distance at different temperatures as interpolated from Ref. [37]

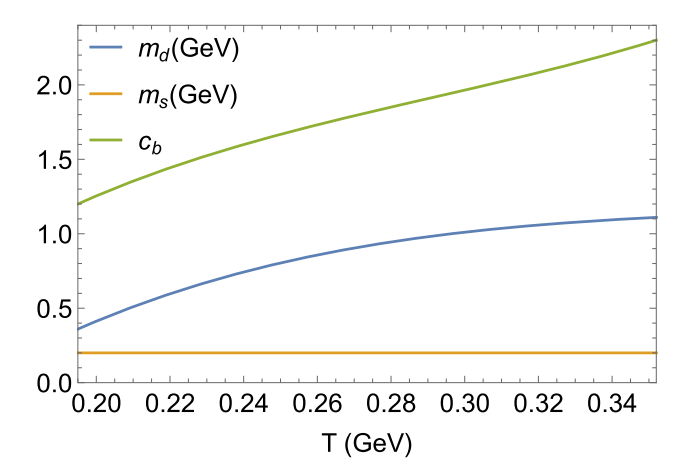


Fig. 4 The in-medium potential parameters as a function of temperature

of temperatures used here) which were based on fits to the IQCD data for HQ free energies, see Fig. 3, but allowing for $\pm~10\%$ variations to illustrate underlying uncertainties. The Φ functions show the qualitatively expected features of amplifying the interference effects deeper into the bound state as temperature increases.

The main difference relative to the previous T-matrix results lies in the screening parameters of the potential as a function of temperature, shown in Fig. 4. Most notably, it turns out that the fits to the WLCs can be carried out with a constant Debye mass for the string interaction, with $m_s = 0.2 \, \text{GeV}$ being comparable to the low-T values in previous work but not increasing with T. Instead, we find that an increase in the c_b parameter is in order (which was assumed to be constant at $c_b = 1.3 - 1.55$ in the previous works), implying that the screening of the string interaction is relegated to larger distances. On the other hand, the screening mass for the color-Coulomb interaction did not change much in either magnitude nor temperature dependence.

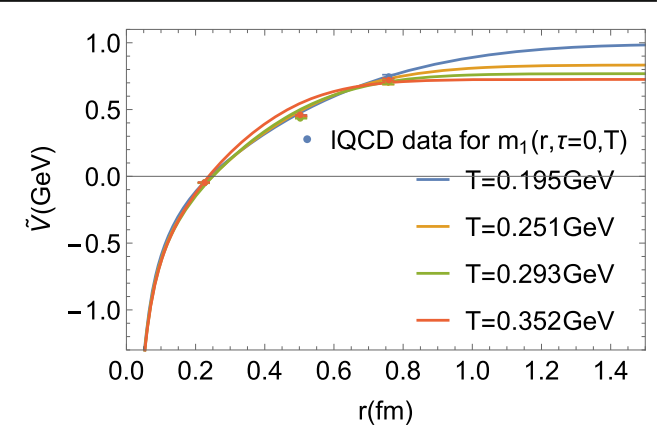


Fig. 5 The in-medium potentials (driving kernels) obtained from the T-matrix approach (lines) as a function of distance at different temperatures in comparison to the 2+1-flavor lQCD results (dots) for the first cumulants of WLCs at $\tau = 0.028 \, \text{fm}$ [29]

The pertinent in-medium potentials are displayed in Fig. 5. Following the discussion of the screening parameters, the main difference to previous T-matrix extractions largely based on HQ free energies lies at the higher temperatures and larger distances where less screening is present based on the WLCs fits. We also plot IQCD data points extracted from the small- τ limit of m_1 . Although they are not necessarily the same quantities (on the lattice one calculates the energy of the static $Q\bar{Q}$ pair) and are based on different underlying spectral functions, they essentially overlap with each other. At the largest temperature, the potentials inferred from the Tmatrix deviate somewhat from the IQCD-based extractions in the interplay of the medium- and large-distance points. This is related to the discrepancy in the WLC fits in lowerright panel in Fig. 2 and might also be in part due to the fact that to observe string breaking on the lattice, it is not sufficient to consider WLCs or Wilson loops alone, but also include operators corresponding to static-light mesons in the analysis [58] (recall our remark following Eq. (12)). On the other hand, the T-matrix based potentials shown in Fig. 5 exhibit essentially no screening for r < 0.8 fm in agreement with recent IQCD findings on the energy of static QQ pair [29,30]. Previous IQCD results with asqtad action and limited statistics resulted in an energy of a static $Q\bar{Q}$ pair that is screened at shorter distances [59]. However, these results are superseded by the ones from Refs. [29,30] using HISQ action and much higher statistics. Using HTL perturbation theoryinspired spectral representations of WLCs one also obtains a screened $Q\bar{Q}$ energy. However, HTL-inspired spectral representations have the screening of the potential built in from the very beginning (and do not account for the string part of the potential). On the other hand, as discussed in Ref. [29], the spectral function in HTL perturbation theory does not describe the lattice QCD results on m_1 . Therefore, the use of



Eur. Phys. J. A (2024) 60:92 Page 7 of 12 92

a HTL-guided form of the spectral function in the analysis of IQCD data is not well motivated.

We also note that our T-matrix fits utilize a mixing coefficient for the vector component of the confining potential of $\chi=0.8$, compared to 0.6 in Ref. [36] and 1 in Ref. [37]. While this choice still takes advantage of the improvement in the hyperfine splittings in the vacuum spectroscopy, it mitigates somewhat the aforementioned problem in the potential at the highest temperature which would be exacerbated for $\chi=0.6$.

The bridge between the underlying potential and the WLCs is provided by the static $Q\bar{Q}$ spectral functions which are obtained from the selfconsistent solutions of the former, subsequently injected into Eq. (9) and then used to compute the pertinent moment; they are depicted in Fig. 6. The effective mass of the $Q\bar{Q}$ state, characterizing the pole position of $\rho_{O\bar{O}}$ at distance r, is largely determined by the potential, V(r) (and identical to the latter in the limit m_1 ($\tau = 0$)). However, they are not exactly the same since the non-zero real part of the $Q\bar{Q}$ selfenergy, $\Sigma_{Q\bar{Q}}$ in Eq. (10), slightly shifts the pole position away from $\widetilde{V}(r)$. Nevertheless, m_1 ($\tau = 0$) remains an indicator of the $Q\bar{Q}$ effective mass, which turns out to be rather temperature-independent as a consequence of the approximately temperature-independent potentials at small and intermediate distances (as shown in Fig. 5). The increase of effective mass with increasing r results from the smaller attraction (less binding) between O and \bar{O} at larger r.

The width of the static spectral function reflects the absorptive part of interaction between $Q\bar{Q}$ and the medium partons and is quantified by the imaginary part of the QQselfenergy, $\Phi(r, T) \text{Im} \Sigma_{O\bar{O}}(E, T)$, in Eq. (10); its dependence on temperature and distance are consistent with the slope of m_1 in Fig. 2, exhibiting a strong broadening with increasing temperature and distance. The dependence on temperature is a consequence of several competing effects: a larger OGP density and less interference tend to increase the width, while a smaller interaction strength with increasing temperatures decreases it. The r-dependence has two basic components, i.e., a long-range force enabling a parton to interact with a larger number of thermal partons in the heat bath, proportional to the volume of the spherical shell which grows as r^2 [60], and the ceasing of interference effects with $\phi(r)$ approaching 1, enabling both Q and \bar{Q} to independently interact with the QGP.

Finally, we display in Fig. 7 the spectral functions of light quarks, gluons and charm quarks as following from the self-consistent T-matrix solution based on the WLC fit. Not surprisingly, the most significant changes are at the two higher temperatures (T = 0.293, 352 GeV) where the interaction strength is larger than before [36]. In the light-parton sector this leads to broader "quasiparticle" peaks and generates

stronger collective modes on the low-energy shoulder of the quasiparticle peaks at zero parton momentum; note that the effective quark mass is around 0.5 GeV while the peaks of the collective mode are located near $\omega \simeq 0.1$ GeV. For the zero-momentum gluon spectral functions at the two higher temperatures, the collective modes emerge near $\omega = 0.2 \, \text{GeV}$, which is not far from gluon condensation. It is this feature that, especially at $T = 0.352 \,\text{GeV}$, prevents us from improving the fit of the WLC, as a stronger input potential at large distances results in an unstable fitting procedure due to the emergence of gluon condensation (signalled by a disappearance of the low-energy peak and a real part of the propagator flipping from negative to positive). Whether this "feature" can be turned into a framework where the bare parton masses are selfconsistently obtained from a condensed ground state is beyond the scope of this work (it would also have to be implemented at the lower temperatures). Even in the charmquark sector the low-momentum spectral functions at the higher temperatures are significantly broader than before, again accompanied with a collective low-energy peak which implies notable deviations from a simple quasiparticle spectral shape.

5 Charm-quark transport coefficients

We are now in position to compute the charm-quark transport properties in the QGP with the refined potential. Two main ingredients to the charm-quark transport coefficients are parton spectral functions, discussed in the previous section, and the heavy-light scattering amplitudes. The latter are displayed in Fig. 8 for S-wave $c\bar{q}$ scattering in the colorsinglet channel (which provides the largest contribution, and together with color-anti-triplet diquark amplitudes makes up the dominant contribution to the transport coefficient). In our recent work [36], we have found that the inclusion of a vector component in the string force (with mixing coefficient $\chi = 0.6$) leads to significantly harder momentum dependence of the scattering amplitudes than the previous results for $\chi = 1$ [37]. This trend persists here, although a little less pronounced due to the choice of $\chi = 0.8$, leading to slightly reduced amplitudes for $T = 0.195 \,\text{GeV}$ (compared to $\chi = 0.6$) while they are quite comparable for T = 0.251 GeV at finite momentum. For the two higher temperatures, the effect of the stronger potential becomes important again.

As the resonance peaks in the heavy-light amplitudes are largely below the "nominal" 2-parton threshold (e.g., $E_{cm} \simeq 2\,\text{GeV}$ for the S-wave "D-meson" resonances in Fig. 8 vs. $E_{\text{thr}} = m_q + m_c \simeq 2.3\,\text{GeV}$ at $T = 0.195\,\text{GeV}$), it is mandatory to account for the nontrivial spectral functions in the evaluation of the HQ transport coefficient. Following the previous study [60] in this context, the off-shell effects in calculating the HQ friction coefficient (relaxation rate) can



92 Page 8 of 12 Eur. Phys. J. A (2024) 60:92

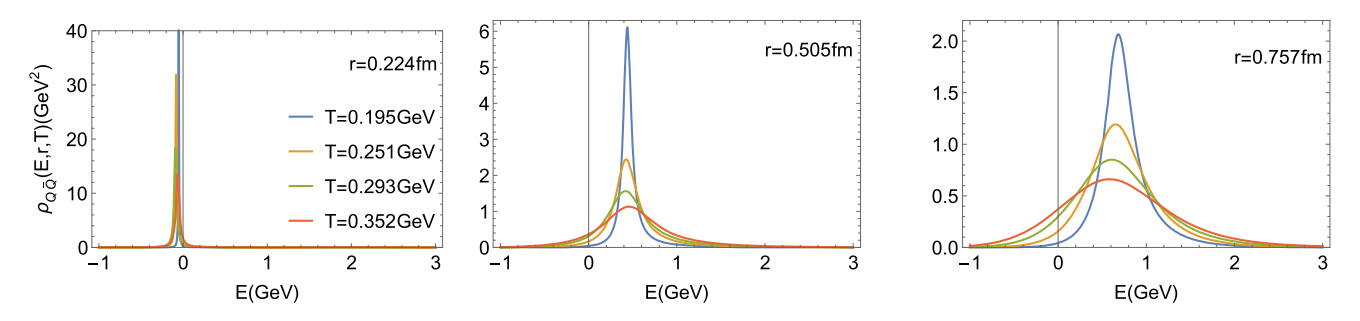


Fig. 6 The spectral functions (with E shifted by twice static-quark mass) of static quark antiquark pair as a function of energy at different temperatures and distances

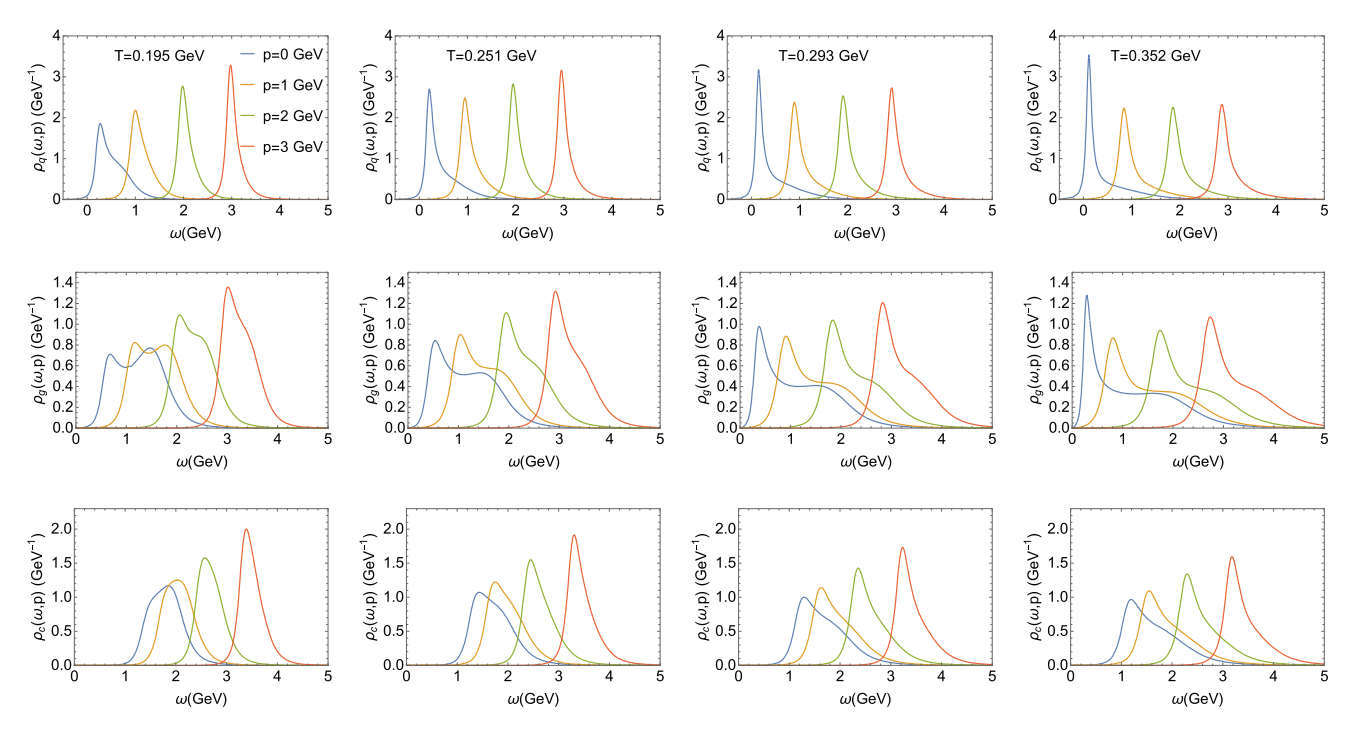


Fig. 7 Single-parton spectral functions for light quarks (first row), gluons (second row) and charm quarks (third row) as a function of energy for various 3-momenta in each panel. From left to right, the four columns correspond to temperatures of $T=0.195,\,0.251,\,0.293$ and $0.352\,\text{GeV}$, respectively

be implemented by utilizing Kadanoff-Baym equations to yield

$$A(p) = \sum_{i} \frac{1}{2\varepsilon_{c}(p)} \int \frac{d\omega' d^{3}\mathbf{p}'}{(2\pi)^{3}2\varepsilon_{c}(p')} \frac{dvd^{3}\mathbf{q}}{(2\pi)^{3}2\varepsilon_{i}(q)} \frac{dv'd^{3}\mathbf{q}'}{(2\pi)^{3}2\varepsilon_{i}(q')}$$

$$\times \delta^{(4)} \frac{(2\pi)^{4}}{d_{c}} \sum_{a,l,s} |M|^{2} \rho_{c}(\omega', p') \rho_{i}(v, q) \rho_{i}(v', q')$$

$$\times \left[1 - n_{c}(\omega')\right] n_{i}(v) \left[1 \pm n_{i}(v')\right] \left(1 - \frac{\mathbf{p} \cdot \mathbf{p}'}{\mathbf{p}^{2}}\right). \tag{15}$$

Here $\delta^{(4)}$ is a short-hand notation for the energy-momentum conserving δ -function in the $2 \rightarrow 2$ scattering process, $d_c = 6$ the spin-color degeneracy of charm quarks, and the summation, \sum_i , is over all light-flavor quarks and gluons making up the thermal medium, $i = u, \bar{u}, d, \bar{d}, s, \bar{s}, g$ (the masses for

light and strange quarks are assumed to be the same). Only the incoming charm quark is taken to be of definite momentum and corresponding on-shell energy, while the off-shell effects are implemented by energy convolutions over the spectral functions of the light parton and the outgoing charm quark. The heavy-light scattering matrix elements, $|M|^2$ in Eq. (15), are directly related to the T-matrix in the CM frame and incorporate the summation over all possible two-body color and partial-wave channels [60].

In Fig. 9 we plot our results for the charm-quark friction coefficient, A(p; T). At the lower two temperatures the WLC-based result is a little lower than the one from Ref. [36], mostly due to the smaller value of χ (0.8 vs. 0.6), but at temperatures $T \gtrsim 0.3$ GeV, it becomes larger at low momentum (due to the stronger potential) and comparable at momenta



Eur. Phys. J. A (2024) 60:92 Page 9 of 12 92

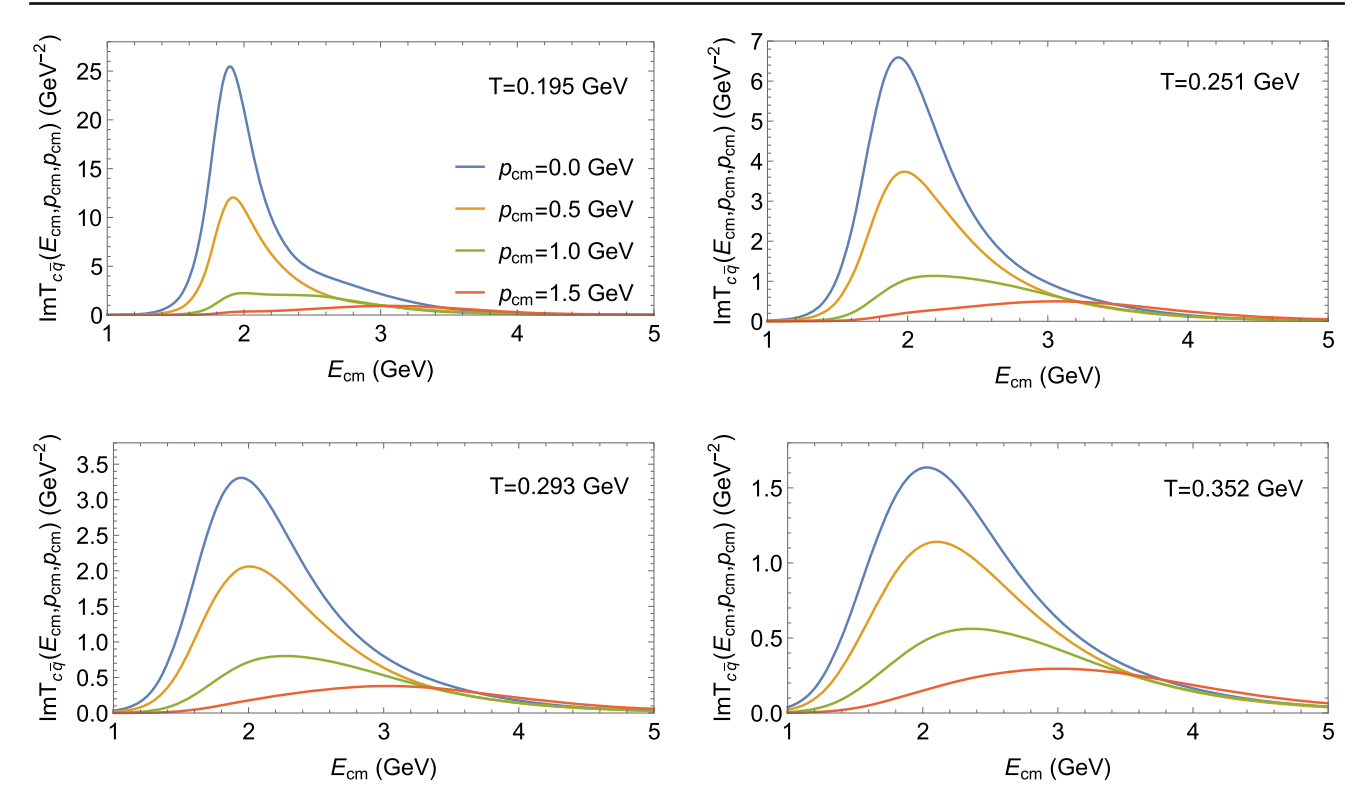


Fig. 8 The imaginary part of the S-wave charm-light T-matrices as a function of CM energy in the color-singlet channel at different temperatures for various CM momenta in each panel

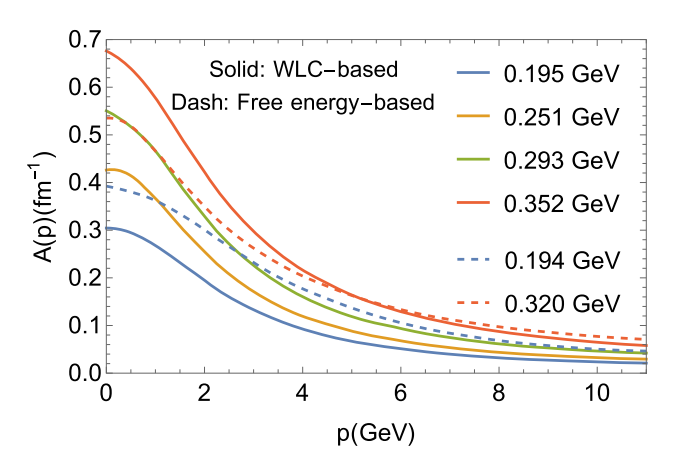


Fig. 9 The charm-quark friction coefficient as a function of charm-quark 3-momentum at different temperatures. The solid lines are the current results based on the constraints from the WLCs, while the dashed lines are largely based on constraints from in-medium HQ free energies [36]

 $p \gtrsim 8~GeV$ (where the color-Coulomb interaction starts to dominate). Based on this comparison to our previous results (which included constraints from the HQ free energy), our conservative estimate of the systematic uncertainty of the T-matrix results for the charm-quark transport coefficient amounts to 20–30%.

The spatial diffusion coefficient, $D_s = T/(M_c A(p=0))$, which is proportional to the relaxation time, $\tau_c = 1/A(p=0)$, is commonly scaled by the inverse thermal wavelength, $2\pi T$, to render a dimensionless quantity. We display the scaled diffusion coefficient in Fig. 10 as a function of temperature. In the static limit our result is in fair agreement with recent IQCD data [51,61], and about a factor of 2–3 larger than the result from the AdS/CFT correspondence which is believed to provide a quantum lower bound for this quantity [62]. The temperature dependence is a bit weaker than our previous results, again a consequence of the stronger potential at the higher temperatures.

The phenomenological consequences of our updated transport coefficients for HF observables in URHICs, which will also require the inclusion of radiative contributions [63], remain to be worked out.

6 Conclusions

We have applied the thermodynamic T-matrix approach to calculate static Wilson line correlators and utilized them to analyze pertinent lattice data. By varying the screening properties of the input potential and carrying out selfconsistent calculations of the 1- and 2-body correlation functions that encompass a description of IQCD results for the QGP



92 Page 10 of 12 Eur. Phys. J. A (2024) 60:92

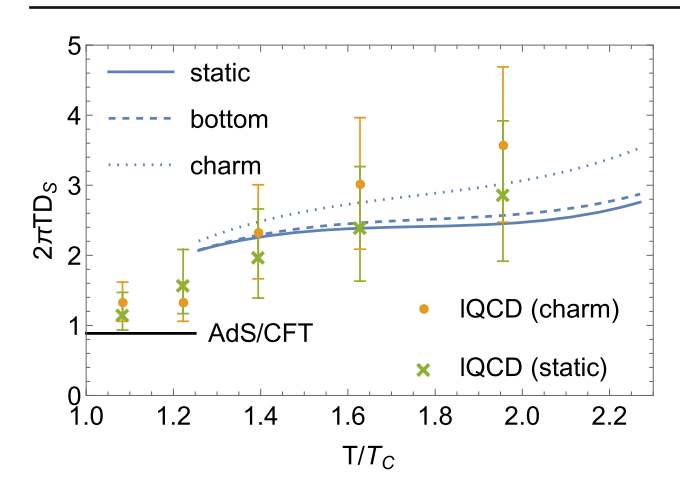
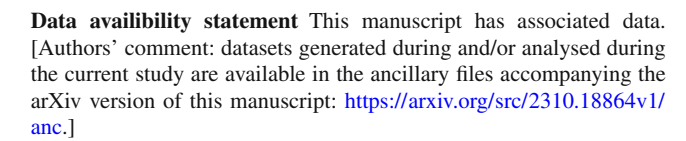


Fig. 10 Our result for the spatial diffusion coefficient for static (blue solid line), bottom (blue dashed line) and charm (blue dotted line) quarks as a function of temperature (scaled by T_c =0.155 GeV) compared to the 2+1-flavor lQCD data [51,61] (yellow dots and green crosses with error bars for charm and static quarks, respectively) and the AdS/CFT estimate [62] (black line). The bare quark masses for charm and bottom are 1.359 and 4.681 GeV, respectively, and we use 10 GeV to approximate the static limit

equation of state, solutions were found that result in a fair agreement with the IQCD data for the first cumulants as a function of euclidean time. While the input potential at low temperatures is quite similar to previous solutions that were based on fits to heavy-quark free energies, more significant adjustments were required at temperatures above $\sim 300\,\mathrm{MeV}$, amounting to a significantly less screened (*i.e.*, stronger) potential. This reinforces earlier findings that remnants of the confining force play a critical role in the properties of the strongly coupled QGP (well) above the critical temperature, with parton collision widths in excess of 0.5 GeV.

An immediate consequence of the stronger potential is an enhancement of low-energy collective modes in the light-quark and gluon spectral functions that develop well below the nominal values of their masses, implying strong deviations from the quasiparticle picture. Even for charm-quark spectral functions this distortion is still significant. We have also computed the pertinent HQ transport coefficients. Their temperature dependence turns out to be more gradual than before, and the predicted spatial diffusion coefficient in the static limit is still in approximate agreement with recent 2+1-flavor lQCD results. It will be interesting to see how these calculations fare when implemented into phenomenological applications to HF data in heavy-ion collisions. Work in this direction is in progress.

Acknowledgements This work has been supported by the U.S. National Science Foundation under Grant Nos. PHY-2209335, PHY-1913286 and by the U.S. Department of Energy, Office of Science, Office of Nuclear Physics through contract No. DE-SC0012704 and the Topical Collaboration in Nuclear Theory on *Heavy-Flavor Theory (HEFTY) for QCD Matter* under award no. DE-SC0023547.



Code availability statement This manuscript has no associated code/software in a data repository. [Author's comment: Not applicable.]

A Relation between first cumulant of WLC and potential

In this Appendix we prove the identity that the first cumulant of the WLCs in the limit of vanishing euclidean time recovers the static potential, $m_1(r, \tau = 0) = \widetilde{V}(r)$ (for simplicity we suppress the temperature dependence), as mentioned at the end of Sect. 3. Expanding $W(r, \tau)$ in the vicinity of $\tau = 0$, one obtains

$$\begin{split} W(r,\tau) &= \int_{-\infty}^{\infty} dE e^{-E\tau} \rho_{Q\bar{Q}} \left(E, r \right) \\ &\approx \int_{-\infty}^{\infty} dE \rho_{Q\bar{Q}} (E,r) - \tau \int_{-\infty}^{\infty} dE E \rho_{Q\bar{Q}} (E,r) \\ &= 1 - \tau \widetilde{V}(r). \end{split} \tag{16}$$

The last identity in Eq. (16) has been proved in Ref. [37] using a contour integral and the fact that the two-body selfenergy, $\Sigma_{Q\bar{Q}}$, in the spectral function, $\rho_{Q\bar{Q}}$ of Eq. (10), is analytic. In addition, the identity $\int_{-\infty}^{\infty} dE \rho_{Q\bar{Q}}(E, r) = 1$ is nothing but the normalization condition of spectral function. The first cumulant of the WLC, $m_1(r, \tau)$, then becomes

$$m_1(r,\tau) = -\partial_\tau \ln W(r,\tau) = \widetilde{V}(r), \tag{17}$$

and all the higher-order terms of τ vanish at $\tau = 0$.

References

- F. Prino, R. Rapp, Open Heavy Flavor in QCD Matter and in Nuclear Collisions. J. Phys. G 43(9), 093002 (2016)
- A. Beraudo et al., Extraction of Heavy-Flavor Transport Coefficients in QCD Matter. Nucl. Phys. A 979, 21–86 (2018)
- X. Dong, V. Greco, Heavy quark production and properties of Quark-Gluon Plasma. Prog. Part. Nucl. Phys. 104, 97–141 (2019)
- R. Rapp, D. Blaschke, P. Crochet, Charmonium and bottomonium production in heavy-ion collisions. Prog. Part. Nucl. Phys. 65, 209– 266 (2010)
- L. Kluberg, H. Satz. Color Deconfinement and Charmonium Production in Nuclear Collisions. (2010)
- P. Braun-Munzinger, J. Stachel, Charmonium from statistical hadronization of heavy quarks—a probe for deconfinement in the quark-gluon plasma. Landolt-Bornstein 23, 424 (2010)
- X. Du, S.Y.F. Liu, R. Rapp, Extraction of the heavy-quark potential from bottomonium observables in heavy-ion collisions. Phys. Lett. B 796, 20–25 (2019)
- F. Karsch, S. Datta, E. Laermann, P. Petreczky, S. Stickan, I. Wetzorke, Hadron correlators, spectral functions and thermal dilepton rates from lattice QCD. Nucl. Phys. A 715, 701–704 (2003)



Eur. Phys. J. A (2024) 60:92 Page 11 of 12 92

S. Datta, F. Karsch, P. Petreczky, I. Wetzorke, Behavior of charmonium systems after deconfinement. Phys. Rev. D 69, 094507 (2004)

- P. Petreczky, K. Petrov, Free energy of a static quark anti-quark pair and the renormalized Polyakov loop in three flavor QCD. Phys. Rev. D 70, 054503 (2004)
- A. Mocsy, P. Petreczky, Heavy quarkonia survival in potential model. Eur. Phys. J. C 43, 77–80 (2005)
- O. Kaczmarek, F. Zantow. Static quark anti-quark interactions in zero and finite temperature QCD. I. Heavy quark free energies, running coupling and quarkonium binding. Phys. Rev. D, 71:114510(2005)
- A. Jakovac, P. Petreczky, K. Petrov, A. Velytsky, Quarkonium correlators and spectral functions at zero and finite temperature. Phys. Rev. D 75, 014506 (2007)
- G. Aarts, C. Allton, M.B. Oktay, M. Peardon, and J.-I. Skullerud. Charmonium at high temperature in two-flavor QCD. Phys. Rev. D, 76:094513 (2007)
- P. Petreczky, On temperature dependence of quarkonium correlators. Eur. Phys. J. C 62, 85–93 (2009)
- G. Aarts, S. Kim, M.P. Lombardo, M.B. Oktay, S.M. Ryan, D.K. Sinclair, J.I. Skullerud, Bottomonium above deconfinement in lattice nonrelativistic QCD. Phys. Rev. Lett. 106, 061602 (2011)
- 17. G. Aarts, C. Allton, S. Kim, M.P. Lombardo, M.B. Oktay, S.M. Ryan, D.K. Sinclair, J.I. Skullerud, What happens to the Υ and η_b in the quark-gluon plasma? Bottomonium spectral functions from lattice QCD. JHEP **11**, 103 (2011)
- H.T. Ding, A. Francis, O. Kaczmarek, F. Karsch, H. Satz, W. Soeldner, Charmonium properties in hot quenched lattice QCD. Phys. Rev. D 86, 014509 (2012)
- 19. S. Kim, P. Petreczky, A. Rothkopf, Lattice NRQCD study of S- and P-wave bottomonium states in a thermal medium with $N_f=2+1$ light flavors. Phys. Rev. D **91**, 054511 (2015)
- A. Bazavov, Yu. Frithjof Karsch, S.M. Maezawa, P. Petreczky, Inmedium modifications of open and hidden strange-charm mesons from spatial correlation functions. Phys. Rev. D 91(5), 054503 (2015)
- Alexei Bazavov, Nora Brambilla, Peter Petreczky, Antonio Vairo, and Johannes Heinrich Weber. Color screening in (2+1)-flavor QCD. Phys. Rev. D, 98(5):054511, (2018)
- R. Larsen, S. Meinel, S. Mukherjee, P. Petreczky, Thermal broadening of bottomonia: Lattice nonrelativistic QCD with extended operators. Phys. Rev. D 100(7), 074506 (2019)
- R. Larsen, S. Meinel, S. Mukherjee, P. Petreczky, Excited bottomonia in quark-gluon plasma from lattice QCD. Phys. Lett. B 800, 135119 (2020)
- R. Larsen, S. Meinel, S. Mukherjee, P. Petreczky, Bethe-Salpeter amplitudes of Upsilons. Phys. Rev. D 102, 114508 (2020)
- Peter Petreczky, Sayantan Sharma, and Johannes Heinrich Weber. Bottomonium melting from screening correlators at high temperature. Phys. Rev. D, 104(5):054511, (2021)
- Ralf Rapp and Hendrik van Hees. Heavy Quarks in the Quark-Gluon Plasma. pages 111–206, (2010)
- A. Mocsy, P. Petreczky, M. Strickland, Quarkonia in the Quark Gluon Plasma. Int. J. Mod. Phys. A 28, 1340012 (2013)
- M. He, H. van Hees, R. Rapp, Heavy-quark diffusion in the quark– gluon plasma. Prog. Part. Nucl. Phys. 130, 104020 (2023)
- Dibyendu Bala, Olaf Kaczmarek, Rasmus Larsen, Swagato Mukherjee, Gaurang Parkar, Peter Petreczky, Alexander Rothkopf, and Johannes Heinrich Weber. Static quark-antiquark interactions at nonzero temperature from lattice QCD. Phys. Rev. D, 105(5):054513, (2022)
- Alexei Bazavov, Daniel Hoying, Olaf Kaczmarek, Rasmus N. Larsen, Swagato Mukherjee, Peter Petreczky, Alexander Rothkopf, and Johannes Heinrich Weber. Un-screened forces in Quark-Gluon Plasma? 8 (2023)

 D. Cabrera, R. Rapp, T-Matrix Approach to Quarkonium Correlation Functions in the QGP. Phys. Rev. D 76, 114506 (2007)

- 32. F. Riek, R. Rapp, Quarkonia and Heavy-Quark Relaxation Times in the Quark-Gluon Plasma. Phys. Rev. C 82, 035201 (2010)
- E. Megias, E. Ruiz Arriola, and L. L. Salcedo. Dimension two condensates and the Polyakov loop above the deconfinement phase transition. JHEP, 01:073, (2006)
- 34. M. Mannarelli, R. Rapp, Hadronic modes and quark properties in the quark-gluon plasma. Phys. Rev. C 72, 064905 (2005)
- F. Riek, R. Rapp, Selfconsistent Evaluation of Charm and Charmonium in the Quark-Gluon Plasma. New J. Phys. 13, 045007 (2011)
- Z. Tang, R. Rapp Spin-dependent interactions and heavy-quark transport in the quark-gluon plasma. Phys. Rev. C. 108(4), 044906 (2023)
- 37. Shuai Y. F. Liu and Ralf Rapp. *T*-matrix Approach to Quark-Gluon Plasma. Phys. Rev. C, 97(3):034918, (2018)
- R. Brockmann, R. Machleidt, The Dirac-Brueckner Approach. Int. Rev. Nucl. Phys. 8, 121–169 (1999)
- M. Cheng et al., The QCD equation of state with almost physical quark masses. Phys. Rev. D 77, 014511 (2008)
- P. Petreczky, Quarkonium in Hot Medium. J. Phys. G 37, 094009 (2010)
- A. Bazavov, Y. Burnier, P. Petreczky, Lattice calculation of the heavy quark potential at non-zero temperature. Nucl. Phys. A 932, 117–121 (2014)
- A. Bazavov et al., Equation of state in (2+1)-flavor QCD. Phys. Rev. D 90, 094503 (2014)
- V.D. Mur, V.S. Popov, Y.A. Simonov, V.P. Yurov, Description of relativistic heavy - light quark - anti-quark systems via Dirac equation. J. Exp. Theor. Phys. 78, 1–14 (1994)
- W. Lucha, F.F. Schoberl, D. Gromes, Bound states of quarks. Phys. Rept. 200, 127–240 (1991)
- N. Brambilla, A. Vairo, Heavy quarkonia: Wilson area law, stochastic vacuum model and dual QCD. Phys. Rev. D 55, 3974–3986 (1997)
- N. Brambilla, A. Vairo, Nonperturbative dynamics of the heavylight quark system in the nonrecoil limit. Phys. Lett. B 407, 167– 173 (1997)
- A.P. Szczepaniak, E.S. Swanson, On the Dirac structure of confinement. Phys. Rev. D 55, 3987–3993 (1997)
- D. Ebert, V. O. Galkin, and R. N. Faustov. Mass spectrum of orbitally and radially excited heavy - light mesons in the relativistic quark model. Phys. Rev. D, 57:5663–5669, 1998. [Erratum: Phys.Rev.D 59, 019902 (1999)]
- 49. D. Ebert, R.N. Faustov, V.O. Galkin, Properties of heavy quarkonia and B_c mesons in the relativistic quark model. Phys. Rev. D **67**, 014027 (2003)
- M. Tanabashi et al., Review of Particle Physics. Phys. Rev. D 98(3), 030001 (2018)
- L. Altenkort, O. Kaczmarek, R. Larsen, S. Mukherjee, P. Petreczky, H.-T. Shu, S. Stendebach, Heavy Quark Diffusion from 2+1 Flavor Lattice QCD with 320 MeV Pion Mass. Phys. Rev. Lett. 130(23), 231902 (2023)
- 52. M. Laine, O. Philipsen, P. Romatschke, M. Tassler, Real-time static potential in hot QCD. JHEP **03**, 054 (2007)
- F. Karsch, E. Laermann, P. Petreczky, S. Stickan, Infinite temperature limit of meson spectral functions calculated on the lattice. Phys. Rev. D 68, 014504 (2003)
- J. M. Luttinger and John Clive Ward. Ground state energy of a many fermion system. 2. Phys. Rev., 118:1417–1427, (1960)
- G. Baym, L.P. Kadanoff, Conservation Laws and Correlation Functions. Phys. Rev. 124, 287–299 (1961)
- G. Baym, Selfconsistent approximation in many body systems. Phys. Rev. 127, 1391–1401 (1962)



92 Page 12 of 12 Eur. Phys. J. A (2024) 60:92

 Shuai Y. F. Liu and Ralf Rapp. Spectral and transport properties of quark–gluon plasma in a nonperturbative approach. Eur. Phys. J. A, 56(2):44, (2020)

- 58. G.S. Bali, H. Neff, T. Duessel, T. Lippert, K. Schilling, Observation of string breaking in QCD. Phys. Rev. D 71, 114513 (2005)
- Y. Burnier, O. Kaczmarek, A. Rothkopf, Static quark-antiquark potential in the quark-gluon plasma from lattice QCD. Phys. Rev. Lett. 114(8), 082001 (2015)
- Shuai Y. F. Liu, Min He, and Ralf Rapp. Probing the in-Medium QCD Force by Open Heavy-Flavor Observables. Phys. Rev. C, 99(5):055201, (2019)
- L. Altenkort, D. de la Cruz, O. Kaczmarek, R. Larsen, G.D. Moore, S. Mukherjee, P. Petreczky, H.-T. Shu, S. Stendebach, Quark Mass Dependence of Heavy Quark Diffusion Coefficient from Lattice QCD. Phys. Rev. Lett. 132(5), 051902 (2024)
- J. Casalderrey-Solana, D. Teaney, Heavy quark diffusion in strongly coupled N=4 Yang-Mills. Phys. Rev. D 74, 085012 (2006)

63. Shuai Y. F. Liu and Ralf Rapp. Nonperturbative Effects on Radiative Energy Loss of Heavy Quarks. JHEP, 08:168, (2020)

Springer Nature or its licensor (e.g. a society or other partner) holds exclusive rights to this article under a publishing agreement with the author(s) or other rightsholder(s); author self-archiving of the accepted manuscript version of this article is solely governed by the terms of such publishing agreement and applicable law.

